Journal of
Marine Science and Engineering

MDPI

Article

Wave Drift Force and Moment in Deep and Shallow Water

Heinrich Söding

Institute for Fluid Dynamics and Ship Theory, Technical University Hamburg, 21073 Hamburg, Germany; h.soeding@tu-harburg.de

Abstract: To attain a low Energy Efficiency Design Index (EEDI), large ships possibly lack the necessary propulsion power to avoid stranding in case of strong adverse wind and wave conditions. To estimate this danger, here, the longitudinal and transverse drift force and the yaw drift moment caused by regular waves of arbitrary frequency and direction are computed using a 3-dimensional Rankine panel method. In many cases, drift forces are larger in shallow than in deep water. Therefore, the theory for computing drift force and moment is extended to shallow water. As published results for shallow water are lacking, the method is verified only for deep water by comparisons with results of model experiments and CFD computations for three ships. For one of them, the dependence of non-dimensional coefficients of longitudinal and transverse drift force and of the drift yaw moment on wave frequency, wave angle, water depth and ship speed is shown. The source files of the programs used for these computations may be obtained from the author if an adequate fee is donated to the Medecins Sans Frontieres or to the author.

Keywords: seakeeping; drift force; shallow water; panel method

1. Motivation

In a heavy seaway, ships may lack the necessary propulsion power to proceed against wind, seaway and current, or to turn into a nautically required direction because of large wind- and wave-induced yaw moments. Therefore, ships near to a coast line have to sail either to a sheltered region or to the open sea before such dangerous conditions occur. Especially since the introduction of the Energy Efficiency Design Index (EEDI), newly built vessels tend to have low propulsion power, thus increasing the danger of stranding [1]. In any case, the master should know in advance the limits of wind velocity and significant wave height for safe ship operation near a coastline [2].

Wind forces and the wind-induced yaw moment on ships can be predicted using wind load coefficients published in the book by Blendermann [3]. They are based on comprehensive wind tunnel tests. An alternative may be computational fluid dynamics (CFD) methods based on solving the Reynolds-Averaged Navier–Stokes (RANS) equations for the air flow around the part of the ship above the water surface.

On the other hand, generally applicable methods for predicting the maneuverability of ships in steep waves, including the danger of broaching-to, are not yet available. However, if broaching-to is excluded, a simpler, moderately accurate, practically useful procedure to predict maneuvering motions in waves was described by Uharek and Cura-Hochbaum [4]. It exploits the fact that changing the ship's course angle takes a lot of time compared to the encounter period of the relevant waves. This simplified procedure consists of the following three steps:

check for updates

Academic Editor: Decheng Wan

Received: 27 October 2024
Revised: 12 December 2024
Accepted: 27 December 2024
Published: 2 January 2025

Citation: Söding, H. Wave Drift Force and Moment in Deep and Shallow Water. *J. Mar. Sci. Eng.* **2025**, *13*, 64. https://doi.org/10.3390/jmse13010064

1. In regular waves of various lengths and directions, the second-order (with respect to wave amplitude) time-averaged wave force and moment are either computed or measured in model tests.
2. To simulate maneuvering in a natural, irregular seaway, the above so-called drift responses are superimposed according to the contribution of each of these regular waves to the assumed wave spectrum. That results in time functions of wave drift force and moment.
3. The time functions, together with maneuvering coefficients determined for the ship in still water, are used to simulate the ship's low-frequency motion for assumed engine and rudder actions.

The present work aims to improve the first of these steps, especially by extending previously developed methods [5] to a more exact treatment of shallow water. That is important because the limiting wind and wave conditions for sufficient maneuverability are most relevant for ships near to a shore. In this paper, potential flow methods with viscous corrections are used because they are more practical than viscous CFD methods: For seakeeping, potential methods appear not inferior with respect to accuracy, and mesh generation and computing times are faster by orders of magnitude.

2. Introduction to Drift Force and Moment

Drift forces are time-averaged wave forces on a body. The negative longitudinal drift force is the wave-induced added resistance. For bodies without forward speed, drift forces act (roughly) in wave propagation direction. For bodies with steady speed ahead, drift forces tend to be directed backward. For surface vessels, normally only the longitudinal and transverse drift force and the yaw drift moment are relevant; the other drift components cause small changes in average draft, heel and trim.

The leading order of drift forces is 2, which means that drift forces are, approximately, proportional to the square of the wave amplitude. Sometimes the expression 'quadratic transfer functions' is used for second-order drift responses per wave amplitude squared. Here, it is shown how second-order drift force and moment can be determined from first-order responses.

Second-order wave responses consist of a stationary and an oscillatory contribution. The former constitutes the drift response; the latter varies periodically with twice the wave encounter frequency and is practically relevant only for vibrations of the elastic ship hull.

In the following, the drift force and moment are determined from zero-order and first-order ship motions and flow potentials. The influence of second-order ship motions and the second-order flow potential on the drift force and moment are estimated to be negligible. On the other hand, the zero-order contribution, i.e., the steady flow around the ship, should not be neglected or approximated by parallel flow, because this would cause substantial inaccuracies. That is also the reason why drift forces computed by strip methods appear, in many cases, too inaccurate for practical application.

Thus, computing the drift force and moment starts here with computing the steady (zeroth-order) flow due to forward speed, followed by computing the first-order sinusoidal flow due to ship motions (radiation flow) and wave diffraction at the hull.

Simplifications will be made in the following by neglecting various small effects:

- Instead of the exact vertical pressure gradient in the stationary flow, the static approximation ρg is used, because inaccuracies of the computed pressure gradient, especially at the bow, may cause large errors in drift force.
- The vertical drift force and the drift trim moment change the average floating position. The effect of this 'wave squat' on the wetted surface and thus the viscous resistance is neglected.

- The change in mean squared relative velocity between fluid and hull due to the orbital fluid motion in the wave changes the friction resistance; this small effect is also neglected.
- For constant ship velocity over ground, the drift motion of fluid particles in a wave changes the relative velocity between ship and fluid and, thus, the ship resistance.
- Except for towed models, the transverse drift force occurring in oblique and transverse waves causes a transverse ship velocity. The resulting increase in resistance is also neglected.

Published papers on drift forces often neglect contributions which are included here; for instance:

- Interaction between the periodical velocity and the stationary disturbance flow due to ship speed
- Changes in the waterline due to steady ship waves and squat
- Shift of ship-fixed points in the inertial system due to squares of rotation angles
- Changes in normal vectors due to squares of rotation angles

The latter two contributions are, however, small.

3. Steady Flow

To take account of the interaction between the steady flow due to forward speed of the ship and the periodical flow in a regular wave, the steady flow is determined first by a three-dimensional Rankine source method realized in the program Pansteady. The method uses a mesh of triangular panels on the ship hull to satisfy the condition of no flux through the hull. On the water surface, a structured mesh of quadrilateral panels (Figure 1) is used to satisfy the kinematic condition (no flux through the surface) and the dynamic condition (atmospheric pressure). The latter condition requires iterative changes in the water surface height in a region around the ship. In case of shallow water, the boundary condition at the water bottom is satisfied by using pairs of sources above and below the water bottom (mirror principle). The radiation condition (far-field ship waves only behind the ship) is satisfied by back-shifting of sources above the water surface by one panel length [6]. The patch method [7] is used because of its higher accuracy compared to the standard panel method; it uses point sources behind instead of distributed sources on the surface, it satisfies the boundary condition on the average over each panel, and it determines the average panel pressure instead of that at a collocation point. Details of the procedure used in older Rankine source programs to determine the steady flow around a moving ship are given in [5].

A number of new features not described in [5] have also been included. Contrary to the much-used older Rankine panel method GLRankine [8], the panel mesh on the hull is not iteratively adapted to the waterline, but remains fixed to the body, only moving in the earth-fixed frame according to the squat. That requires to deal with partly submerged hull panels. For integrating the pressure over the hull, only the submerged part of such panels is taken into account. For determining the source strengths, it would be inaccurate to use the possibly narrow regions between the lower panel boundary and the waterline directly as a modified hull panel; instead, the flux through the total panel is not made to vanish, but only reduced according to the ratio of the submerged panel area over the total panel area.

Water surface panels immediately behind an immersed transom require also special treatment. Because of the back-shifting of sources above the free surface, directly above these panels there is space for additional sources. These are used to approximately satisfy the condition that the hull pressure at the transom contour should be equal to atmospheric pressure. This holds if the ship speed is sufficiently high to attain a smooth flow separation

at the transom contour; for lower speed, panels arranged on the transom area are taken into account to satisfy the normal no-flux condition.

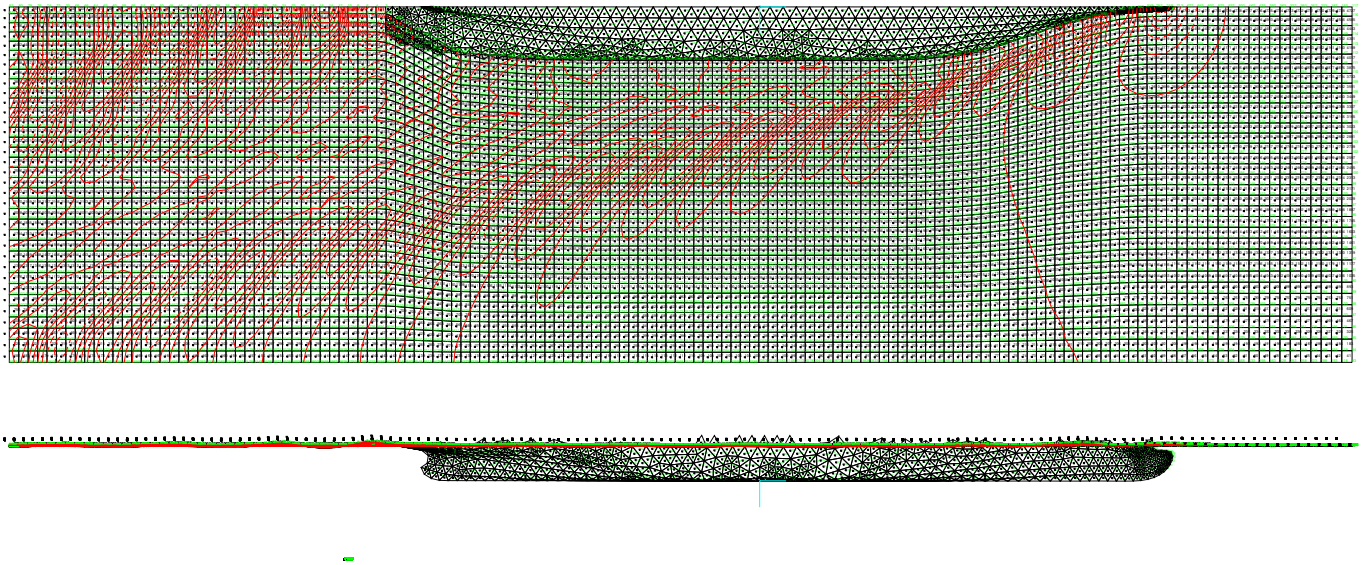

Figure 1. Panel mesh on hull and water surface, source points (black) and surface height contours (red) for computing the steady flow around the 6500-TEU containership at 15 kn speed using program Pansteady.

For Froude numbers below 0.14, the number of panels on the water surface would be too large to resolve the short steady ship waves; that would lead to divergence of the iteration. In this case, the deformation of the water surface and the squat are neglected. The resulting double-body flow could be modeled by using pairs of sources above and below the water surface. However, in case of shallow water, sources arranged symmetrically to both water surface and water bottom would require, in principle, an infinite number of sources for each panel. To avoid that complication, the condition at the water surface is satisfied like for higher Froude numbers by a panel mesh, modifying only the free-surface condition and omitting the deformation of the water surface and the iteration.

4. Periodical Flow

The periodical flow around ships in regular waves is also determined using a Rankine source method. The program Pandfds used for this task applies the same panel mesh on the hull as the program for steady flow. Also, the general structure of the panel mesh on the water surface is the same; however, the mesh extension and fineness are determined depending on the length of the incoming waves. The steady surface deformation is interpolated from the steady panel mesh to that for periodical flow. The magnitude of the steady flow speed on the water surface follows from the height of the surface, and its direction is assumed parallel to the longitudinal panel boundaries. On the hull, on the other hand, the steady flow potential and its gradient are directly used as computed by the program Pansteady. For computing the periodic flow, there is no back-shift of sources above the free-surface panels; instead, the periodic disturbance of the incoming waves, which is modeled by source distributions for diffraction and radiation, is damped by specifying a modified boundary condition on the water surface. This is necessary to avoid wave reflections at the outer boundary of the panel mesh on the water surface. Because equations for determining complex amplitudes are linearized with respect to wave and ship motion amplitudes, no iteration is required here. These and many other details of the method are described in [5].

In many panel methods for seakeeping, the steady flow potential is assumed to be time-independent in an inertial frame. As the ship is moving relative to that potential field, to determine the first-order flow speed and pressure on the hull requires the computation of the Hesse matrix, i.e., the matrix of second derivatives, of the steady flow potential. As panel methods approximate the flow velocities correctly only at one point within each panel (in usual panel methods) or on the average over each panel (in the patch method), the Hesse matrix of the stationary flow potential cannot be determined as the analytical derivative of the flow speed; instead it is approximated by finite-differences (see Appendix A). This causes inaccuracies of the computed motion and load amplitudes. To reduce them, Hachmann [9] proposed to let the steady flow potential field (but not the fluid!) move as fixed to the ship. The effect of this 'Hachmann method' is such that the Hesse matrix is not required to satisfy the body boundary condition, but instead for the condition on the water surface. It turns out that this reduces these inaccuracies effectively. Thus, the Hachmann method is applied here. (For computing the second-order drift force, the Hesse matrix must be determined also on the wetted hull; nonetheless, applying the Hachmann method appears worthwhile.).

Von Graefe [10] pointed out that, if the Hachmann method is used in case of shallow water, the mirror sources below the water bottom must perform vertical motions of opposite sign compared to the ship motions to satisfy the condition of no flux through the water bottom. To take account of that, the stationary disturbance potential must be split into two different parts, ϕ_0 and ψ_0, generated by the sources above and below the water bottom, respectively.

5. Computing Drift Force and Moment

5.1. Preliminaries

For computing drift forces, two Cartesian coordinate systems are used: An inertial system the axes of which are directed forward (x), to starboard (y) and vertically downward (z); and a ship-fixed system $\underline{x}$, $\underline{y}$, $\underline{z}$, which coincides with the inertial system if the ship is in equilibrium floating position in still water. In case of shallow water, also a 'dot coordinate system' $\dot{x}$, $\dot{y}$, $\dot{z}$ is required. Points having fixed coordinates $\dot{x}$, $\dot{y}$, $\dot{z}$ in the dot system are moving in the inertial system like ship-fixed points in horizontal direction, and opposite to ship-fixed points in vertical direction. In still water, the origins of all three systems are the same.

The relation between the coordinates of a point expressed in the ship-fixed coordinate system, $\vec{\underline{x}} = (\underline{x}, \underline{y}, \underline{z})^T$, and the same point expressed in the inertial system, $\vec{x} = (x, y, z)^T$, is

$$\vec{x} = \vec{\underline{x}} + \vec{u} + (T - E)\vec{\underline{x}}. \tag{1}$$

Here, $\vec{u}$ is the vector of ship translations surge, sway, heave. E is the 3 by 3 unit matrix. The matrix T, which takes account of the rotation of the ship relative to the inertial system, has often been published (e.g., in [5]):

$$T = \begin{pmatrix} \cos\psi\cos\theta & \cos\psi\sin\theta\sin\varphi - \sin\psi\cos\varphi & \cos\psi\sin\theta\cos\varphi + \sin\psi\sin\varphi \\ \sin\psi\cos\theta & \sin\psi\sin\theta\sin\varphi + \cos\psi\cos\varphi & \sin\psi\sin\theta\cos\varphi - \cos\psi\sin\varphi \\ -\sin\theta & \cos\theta\sin\varphi & \cos\theta\cos\varphi \end{pmatrix}. \tag{2}$$

It depends on the right-hand rotations about the three axes: roll angle φ, pitch angle θ, and yaw angle ψ.

Equations (1) and (2) are developed into terms of zeroth, first and second order in wave and motion amplitudes. This results in

$$\vec{x} = \underline{\vec{x}} + \vec{u} + \vec{\alpha} \times \underline{\vec{x}} + T_2 \underline{\vec{x}}, \tag{3}$$

where $\vec{\alpha} = (\varphi, \theta, \psi)^T$ is the vector of ship rotations, and T_2 is the second-order part of T:

$$T_2 = \begin{pmatrix} -\frac{1}{2}\theta^2 - \frac{1}{2}\psi^2 & \varphi\theta & \varphi\psi \\ 0 & -\frac{1}{2}\varphi^2 - \frac{1}{2}\psi^2 & \theta\psi \\ 0 & 0 & -\frac{1}{2}\varphi^2 - \frac{1}{2}\theta^2 \end{pmatrix}. \tag{4}$$

Here, and in the following, terms of higher than second order are omitted without notice.

Correspondingly, the relation between the inertial and the dot coordinates of the same point is

$$\vec{x} = \dot{\vec{x}} + \dot{\vec{u}} + \dot{\vec{\alpha}} \times \dot{\vec{x}} + \dot{T}_2 \dot{\vec{x}} \tag{5}$$

with

$$\dot{\vec{x}} = (\dot{x}, \dot{y}, \dot{z})^T, \quad \dot{\vec{u}} = (u_x, u_y, -u_z)^T, \quad \dot{\vec{\alpha}} = (-\varphi, -\theta, \psi)^T, \tag{6}$$

and

$$\dot{T}_2 = \begin{pmatrix} -\frac{1}{2}\theta^2 - \frac{1}{2}\psi^2 & \varphi\theta & -\varphi\psi \\ 0 & -\frac{1}{2}\varphi^2 - \frac{1}{2}\psi^2 & -\theta\psi \\ 0 & 0 & -\frac{1}{2}\varphi^2 - \frac{1}{2}\theta^2 \end{pmatrix}. \tag{7}$$

In the following, normal vectors on a body panel (directed into the body) are scaled so that their magnitude equals the panel area. Corresponding to (3), a panel normal vector expressed in the inertial frame follows from $\underline{\vec{n}}$ (expressed in the body-fixed coordinate system):

$$\vec{n} = \underbrace{\underline{\vec{n}}}_{\vec{n}_0} + \underbrace{\vec{\alpha} \times \underline{\vec{n}}}_{\vec{n}_1} + \underbrace{T_2 \underline{\vec{n}}}_{\vec{n}2}. \tag{8}$$

The sinusoidal dependence on time of first-order quantities like $\vec{u}$ and $\vec{\alpha}$ will be characterized by complex amplitudes designated by $\hat{}$:

$$\vec{u}(t) = \mathrm{Re}(\hat{\vec{u}} e^{i\omega_e t}) \quad \text{and} \quad \vec{\alpha}(t) = \mathrm{Re}(\hat{\vec{\alpha}} e^{i\omega_e t}). \tag{9}$$

The product of two harmonically oscillating quantities $a = \mathrm{Re}(\hat{a} e^{i\omega_e t})$ and $b = \mathrm{Re}(\hat{b} e^{i\omega_e t})$ consists of a constant and a time-dependent part oscillating with twice the frequency of the factors:

$$\begin{aligned} ab &= \mathrm{Re}(\hat{a} e^{i\omega_e t}) \cdot \mathrm{Re}(\hat{b} e^{i\omega_e t}) = \mathrm{Re}[\hat{a} e^{i\omega_e t} \cdot \mathrm{Re}(\hat{b} e^{i\omega_e t})] \\ &= \mathrm{Re}\left[\hat{a} e^{i\omega_e t} \cdot \frac{1}{2}(\hat{b} e^{i\omega_e t} + \hat{b}^* e^{-i\omega_e t})\right] = \frac{1}{2}\mathrm{Re}\left[\hat{a}\hat{b} e^{2i\omega_e t} + \hat{a}\hat{b}^*\right], \end{aligned} \tag{10}$$

where $*$ indicates the complex conjugate. The oscillating part has a time average of zero; thus, the average of the product (indicated here and in the following by over-lining) is

$$\overline{ab} = \frac{1}{2}\mathrm{Re}(\hat{a}\hat{b}^*). \tag{11}$$

Corresponding rules hold for the scalar and the vector product of harmonically oscillating vectors; e.g.,

$$\overline{\vec{a} \times \vec{b}} = \frac{1}{2}\mathrm{Re}(\hat{\vec{a}} \times \hat{\vec{b}}^*). \tag{12}$$

The shift of a ship-fixed point in the inertial system is, according to (3),

$$\vec{v}(\underline{\vec{x}}) = \vec{x} - \underline{\vec{x}} = \underbrace{\vec{u} + \vec{\alpha} \times \underline{\vec{x}}}_{\vec{v}_1(\underline{\vec{x}})} + T_2\underline{\vec{x}}. \tag{13}$$

$\vec{v}_1$ and $T_2\underline{\vec{x}}$ are the first- and second-order contributions at ship-fixed points, respectively. Using the identity

$$-\vec{\alpha} \times (\vec{\alpha} \times \vec{x}) + T_2\vec{x} = -T_2^T\vec{x}, \tag{14}$$

$\vec{v}$ can also be expressed as a function of $\vec{x}$ instead of $\underline{\vec{x}}$:

$$\vec{v}(\vec{x}) = \vec{u} + \vec{\alpha} \times (\vec{x} - \vec{u}) - T_2^T\vec{x}. \tag{15}$$

In the following, the dependence of quantities on $\underline{\vec{x}}$ or $\vec{x}$ is omitted in second-order terms because the difference is a term of third order. Further, the dependence of quantities on t is not noted.

If a quantity depends on both time and space, one has to distinguish partial time derivatives for fixed $\vec{x}$ from those for fixed $\underline{\vec{x}}$. In the following, $\dot{}$ indicates a time derivative for constant $\underline{\vec{x}}$, and $\breve{}$ that for constant $\vec{x}$.

Several expressions depending on $\vec{v}$, which are required later, will now be given:

$$\nabla\vec{v}_1 = \left(\frac{\partial\vec{v}_1}{\partial x}, \frac{\partial\vec{v}_1}{\partial y}, \frac{\partial\vec{v}_1}{\partial z}\right) = \begin{pmatrix} 0 & -\psi & \theta \\ \psi & 0 & -\varphi \\ -\theta & \varphi & 0 \end{pmatrix} = \alpha^T \times E; \tag{16}$$

$$\nabla\breve{\vec{v}}_1 = \dot{\alpha}^T \times E; \tag{17}$$

$$(\nabla\vec{v}_1)\vec{v}_1 = \vec{\alpha} \times \vec{v}_1 = \vec{\alpha} \times (\vec{u} + \vec{\alpha} \times \vec{x}); \tag{18}$$

$$(\nabla\breve{\vec{v}}_1)\vec{v}_1 = \dot{\vec{\alpha}} \times (\vec{u} + \vec{\alpha} \times \vec{x}); \tag{19}$$

$$\breve{\vec{v}}(\underline{\vec{x}}) = \frac{\partial}{\partial t}[\vec{u} + \vec{\alpha} \times (\vec{x} - \vec{u} - \vec{\alpha} \times \vec{x}) + T_2\vec{x}] = \dot{\vec{u}} + \dot{\vec{\alpha}} \times \vec{x} - \frac{\partial}{\partial t}[\vec{\alpha} \times (\vec{u} + \vec{\alpha} \times \vec{x})] + \dot{T}_2\vec{x}. \tag{20}$$

Second-order terms the time average of which is zero will be omitted here and in the following, because they do not contribute to the drift (i.e., time-averaged) force and moment. That applies to the last two terms in (20), because $\vec{\alpha} \times (\vec{u} + \vec{\alpha} \times \vec{x})$ and $T_2\vec{x}$ are, for fixed $\vec{x}$, periodic in time. Thus,

$$\breve{\vec{v}}(\underline{\vec{x}}) = \dot{\vec{u}} + \dot{\vec{\alpha}} \times \vec{x} = \breve{\vec{v}}_1(\vec{x}). \tag{21}$$

5.2. Drift Force and Moment Due to Pressure Acting on the Surface up to the Mean Waterline

The fluid pressure $p(\vec{x}, t)$ acting at $\vec{x}$ at time t generates the following force contribution A:

$$\vec{F}_A = \sum_{panels} p(\underline{\vec{x}}, t)\vec{n}(t). \tag{22}$$

The time functions p and $\vec{n}$ will now be subdivided into contributions of zeroth, first and second order regarding their variation at ship-fixed points:

$$\vec{F}_A = \sum_{panels} (p_0 + p_1 + p_2)(\vec{n}_0 + \vec{n}_1 + \vec{n}_2), \tag{23}$$

where the normal vectors are given by (8). Here, we are interested in the wave-induced drift force, which is the time average of the second-order force $\vec{F}_A^{(2)}$. It follows from (23) as

$$\vec{F}_A^{(2)} = \sum_{panels} (p_0\vec{n}_2 + p_1\vec{n}_1 + p_2\vec{n}_0). \tag{24}$$

Correspondingly for the moment $\vec{M}_A$ around the center of gravity of ship mass G:

$$\begin{aligned} \vec{M}_A &= \sum_{panels} p(\vec{x},t)(\vec{x}-\vec{x}_G)\times\vec{n}(t) && (25)\\ &= \sum_{panels} (p_0+p_1+p_2)[\underline{\vec{x}}-\underline{\vec{x}}_G+\vec{\alpha}\times(\underline{\vec{x}}-\underline{\vec{x}}_G)+T_2(\underline{\vec{x}}-\underline{\vec{x}}_G)]\times(\vec{n}_0+\vec{n}_1+\vec{n}_2). && (26)\end{aligned}$$

Collecting the second-order terms and using (8) gives

$$\begin{aligned}\vec{M}_A^{(2)} = \sum_{panels}\Bigg(& p_0(\underline{\vec{x}}-\underline{\vec{x}}_G)\times(T_2\underline{\vec{n}}) + p_0[\vec{\alpha}\times(\underline{\vec{x}}-\underline{\vec{x}}_G)]\times[\vec{\alpha}\times\underline{\vec{n}}] + p_0[T_2(\underline{\vec{x}}-\underline{\vec{x}}_G)]\times\underline{\vec{n}}\\ & + \underbrace{p_1(\underline{\vec{x}}-\underline{\vec{x}}_G)\times(\vec{\alpha}\times\underline{\vec{n}}) + p_1[\vec{\alpha}\times(\underline{\vec{x}}-\underline{\vec{x}}_G)]\times\underline{\vec{n}}}_{p_1\vec{\alpha}\times[(\underline{\vec{x}}-\underline{\vec{x}}_G)\times\underline{\vec{n}}]} + p_2(\underline{\vec{x}}-\underline{\vec{x}}_G)\times\underline{\vec{n}}\Bigg). \end{aligned} \tag{27}$$

The pressure follows from Bernoulli's equation

$$\frac{p(\vec{x},t)}{\rho} = \frac{1}{2}U^2 - \breve{\phi}(\vec{x},t) + g(z+d) - \frac{1}{2}|\nabla\phi(\vec{x},t)|^2. \tag{28}$$

U is ship speed, d is draft, here defined as depth of the coordinate origin below the still water surface. The flow potential ϕ is superimposed according to the Hachmann method for shallow water:

$$\phi(\vec{x},t) = -Ux + \phi_0(\underline{\vec{x}}) + \psi_0(\dot{\vec{x}}) + \phi_1(\vec{x}). \tag{29}$$

ϕ_0 and ψ_0 together constitute the stationary disturbance potential: functions which are independent of time in coordinate systems $\underline{\vec{x}}$ and $\dot{\vec{x}}$, respectively. In (28), we have to insert them dependent on the inertial location $\vec{x}$. Thus, a Taylor expansion of $\phi_0(\underline{\vec{x}})$ and $\psi_0(\dot{\vec{x}})$ up to second order is made:

$$\phi(\vec{x},t) = -Ux + \phi_0(\vec{x}) + \psi_0(x) - \vec{v}(\vec{x},t)\nabla\phi_0(\vec{x}) - \dot{\vec{v}}(\vec{x},t)\nabla\psi_0(\vec{x}) + \frac{1}{2}\vec{v}^T(\nabla\nabla\phi_0)\vec{v} + \frac{1}{2}\dot{\vec{v}}^T(\nabla\nabla\psi_0)\dot{\vec{v}} + \phi_1(\vec{x}). \tag{30}$$

∇ comprises partial space derivatives in the inertial coordinate directions. Thus, the partial time derivative of ϕ for fixed $\vec{x}$ follows as

$$\begin{aligned}\breve{\phi}(\vec{x},t) &= -\breve{\vec{v}}(\vec{x},t)\nabla\phi_0(\vec{x}) - \breve{\dot{\vec{v}}}(\vec{x},t)\nabla\psi_0(\vec{x}) + \breve{\vec{v}}^T(\nabla\nabla\phi_0)\vec{v} + \breve{\dot{\vec{v}}}^T(\nabla\nabla\psi_0)\dot{\vec{v}} + \breve{\phi}_1(\vec{x})\\ &= -\breve{\vec{v}}(\vec{x},t)\nabla\phi_0(\underline{\vec{x}}) - \breve{\dot{\vec{v}}}(\vec{x},t)\nabla\psi_0(\dot{\vec{x}}) + \breve{\phi}_1(\vec{x})\\ &= -\breve{\vec{v}}(\vec{x},t)(\underline{\nabla}+\vec{\alpha}\times\underline{\nabla})\phi_0(\underline{\vec{x}}) - \breve{\dot{\vec{v}}}(\vec{x},t)(\dot{\nabla}+\vec{\alpha}\times\dot{\nabla})\psi_0(\dot{\vec{x}}) + \breve{\phi}_1(\vec{x}), \end{aligned} \tag{31}$$

where $\underline{\nabla}$ designates derivatives in the directions of the ship-fixed coordinates. The operators $\underline{\nabla}$ and $\dot{\nabla}$ are related by

$$\nabla = \underline{\nabla} + \vec{\alpha}\times\underline{\nabla} + T_2\underline{\nabla} = \dot{\nabla} + \vec{\alpha}\times\dot{\nabla} + \underset{\cdot}{T}_2\dot{\nabla}. \tag{32}$$

Because (24) and (27) require to separate the pressure into orders zero, one and two at ship-fixed points, $\vec{x}$ is changed to $\underline{\vec{x}}$ on the right-hand side of (31) using a Taylor expansion:

$$\breve{\phi}(\vec{x},t) = -\breve{\vec{v}}(\underline{\vec{x}},t)(\underline{\nabla} + \vec{\alpha}\times\nabla)\phi_0(\underline{\vec{x}}) - \underbrace{(\nabla\breve{\vec{v}}\,\vec{v})}_{\dot{\vec{\alpha}}\times\vec{v}_1}\nabla\phi_0$$

$$-\breve{\vec{v}}(\underline{\vec{x}},t)(\dot{\nabla} + \dot{\vec{\alpha}}\times\nabla)\psi_0(\dot{\vec{x}}) - \underbrace{(\nabla\breve{\vec{v}}\vec{v})}_{\dot{\vec{\alpha}}\times\vec{v}_1}\nabla\psi_0 + \breve{\phi}_1(\underline{\vec{x}}) + \nabla\breve{\phi}_1\vec{v}, \tag{33}$$

where (18) and (19) have also been used.

To evaluate (28), we need also $\nabla\phi(\vec{x},t)$. It follows from (30) and from Taylor developments (here up to second order) to change from $\vec{x}$ and $\dot{\vec{x}}$ to $\underline{\vec{x}}$ and from ∇ and $\dot{\nabla}$ to $\underline{\nabla}$:

$$\begin{aligned}
\nabla\phi(\vec{x},t) &= (-U,0,0) + \nabla\phi_0(\underline{\vec{x}}) + \nabla\psi_0(\dot{\vec{x}}) + \nabla\phi_1(\vec{x}) \\
&= (-U,0,0) + (\underline{\nabla} + \vec{\alpha}\times\underline{\nabla} + T_2\underline{\nabla})\phi_0(\underline{\vec{x}}) \\
&\quad +(\dot{\nabla} + \dot{\vec{\alpha}}\times\dot{\nabla} + \dot{T}_2\dot{\nabla})\left[\psi_0(\dot{\vec{x}}) + (\nabla\psi_0)(\vec{v}-\dot{\vec{v}}) + \frac{1}{2}(\vec{v}_1-\dot{\vec{v}}_1)(\nabla\nabla\psi_0)(\vec{v}_1-\dot{\vec{v}}_1)\right] \\
&\quad +\nabla\phi_1(\underline{\vec{x}}) + (\nabla\nabla\phi_1)\vec{v}_1,
\end{aligned} \tag{34}$$

where $\vec{v} = \vec{v}_1 + T_2\underline{\vec{x}}$ and $\dot{\vec{v}} = \dot{\vec{v}}_1 + \dot{T}_2\underline{\vec{x}}$ contain first- and second-order parts. Collecting terms of order 0, 1 and 2 designated as $\vec{w}_0$, $\vec{w}_1$ and $\vec{w}_2$, respectively, gives

$$\nabla\phi(\vec{x},t) = \vec{w}_0 + \vec{w}_1 + \vec{w}_2 \tag{35}$$

with

$$\vec{w}_0 = (-U,0,0) + \underline{\nabla}\phi_0(\underline{\vec{x}}) + \dot{\nabla}\psi_0(\underline{\vec{x}}), \tag{36}$$

$$\vec{w}_1 = \vec{\alpha}\times\underline{\nabla}\phi_0(\underline{\vec{x}}) + (\dot{\nabla}\nabla\psi_0)(\vec{v}_1-\dot{\vec{v}}_1) + (\vec{\alpha}-\dot{\vec{\alpha}})\times\nabla\psi_0 + \dot{\vec{\alpha}}\times\dot{\nabla}\psi_0(\underline{\vec{x}}) + \nabla\phi_1(\underline{\vec{x}}), \tag{37}$$

and

$$\begin{aligned}
\vec{w}_2 &= T_2\underline{\nabla}\phi_0 + \dot{T}_2\dot{\nabla}\psi_0 + \dot{\vec{\alpha}}\times[(\nabla\psi_0)^T(\nabla\vec{v}_1 - \nabla\dot{\vec{v}}_1)] + (\dot{\nabla}\nabla\psi_0)(T_2-\dot{T}_2)\underline{\vec{x}} + (\nabla\psi_0)^T(T_2-\dot{T}_2) \\
&\quad +\frac{1}{2}(\vec{\alpha}+\dot{\vec{\alpha}})\times[(\nabla\nabla\psi_0)(\vec{v}_1-\dot{\vec{v}}_1)] + \frac{1}{2}(\vec{v}_1-\dot{\vec{v}}_1)^T(\nabla\nabla\psi_0)(\nabla\vec{v}_1 - \nabla\dot{\vec{v}}_1) + (\nabla\nabla\phi_1)\vec{v}_1.
\end{aligned} \tag{38}$$

Using the abbreviations $\vec{w}_i$, $i = 1$ to 3, the last term in (28) becomes

$$\frac{1}{2}|\nabla\phi(x,t)|^2 = \frac{1}{2}\nabla\phi\nabla\phi = \frac{1}{2}(\vec{w}_0+\vec{w}_1+\vec{w}_2)(\vec{w}_0+\vec{w}_1+\vec{w}_2) = \frac{1}{2}\vec{w}_0^2 + \vec{w}_0\vec{w}_1 + \vec{w}_0\vec{w}_2 + \frac{1}{2}\vec{w}_1^2. \tag{39}$$

Evaluating the quantity $\dot{\nabla}\psi_0(\underline{\vec{x}})$ in $\vec{w}_0$ may appear problematically because, instead, the quantity $\dot{\nabla}\psi_0(\dot{\vec{x}})$ is read by the program, and there is no obvious possibility to change between these two quantities. However, $\vec{w}_0$ will be multiplied by the second-order quantity $\vec{n}_2$ for determining the drift force. Thus, the difference between both expressions, which is of first-order, would result in a third-order contribution to the drift force and can be neglected. The same holds for other terms involving ψ_0 in (37) and (38).

The different orders of the pressure, again at ship-fixed points, follow from (28), (33) and (36) to (39):

$$\frac{p_0}{\rho} = g(\underline{z}+d) + \frac{1}{2}(U^2 - \vec{w}_0^2); \tag{40}$$

$$\frac{p_1}{\rho} = \breve{\vec{v}}_1 \nabla \phi_0 + \breve{\vec{v}}_{\cdot 1} \nabla \psi_0 - \breve{\phi}_1 + (0,0,g)\vec{v}_1 - \vec{w}_0 \vec{w}_1; \tag{41}$$

$$\frac{p_2}{\rho} = (\vec{\alpha} \times \nabla \phi_0)\breve{\vec{v}}_1 + (\vec{\alpha} \times \nabla \psi_0)\breve{\vec{v}}_{\cdot 1}) + (\dot{\vec{\alpha}} \times \vec{v}_1)\nabla \phi_0 + (\dot{\vec{\alpha}} \times \vec{v}_1)\nabla \psi_0$$

$$-\nabla \breve{\phi}_1 \vec{v}_1 + (0,0,g)(T_2 \underline{x}) - \vec{w}_0 \vec{w}_2 - \frac{1}{2}|\vec{w}_1|^2. \tag{42}$$

The time averages of the first and third term in (42) are the same.

To determine the time average of $\vec{F}_A^{(2)}$, we need the complex amplitude of p_1/ρ,

$$\frac{\hat{p}_1}{\rho} = i\omega_e \hat{\vec{v}}_1 \underline{\nabla} \phi_0 + i\omega_e \hat{\vec{v}}_{\cdot 1} \nabla \psi_0 - i\omega_e \hat{\phi}_1 + (0,0,g)\hat{\vec{v}}_1 - \vec{w}_0 \hat{\vec{w}}_1, \tag{43}$$

where

$$\hat{\vec{w}}_1 = \hat{\vec{\alpha}} \times (\underline{\nabla} \phi_0 + \nabla \psi_0) + (\nabla \nabla \psi_0)(\hat{\vec{v}}_1 - \hat{\vec{v}}_{\cdot 1}) + \nabla \hat{\phi}_1; \tag{44}$$

and the time average of p_2/ρ,

$$\frac{\bar{p}_2}{\rho} = -\frac{1}{2}\mathrm{Re}\left(2i\omega_e(\hat{\vec{\alpha}} \times \underline{\nabla} \phi_0)\hat{\vec{v}}_1^* + i\omega_e(\hat{\vec{\alpha}} \times \nabla \psi_0)(\hat{\vec{v}}_1^* + \hat{\vec{v}}_{\cdot 1}^*) + i\omega_e \underline{\nabla} \hat{\phi}_1 \hat{\vec{v}}_1^* + \frac{1}{2}\hat{\vec{w}}_1 \hat{\vec{w}}_1^*\right) + (0,0,g)(\bar{T}_2 \underline{\vec{x}}) - \vec{w}_0 \bar{\vec{w}}_2. \tag{45}$$

The time average $\bar{T}_2$ follows from (4) as

$$\bar{T}_2 = \begin{pmatrix} -\frac{1}{4}(\hat{\theta}\hat{\theta}^* + \hat{\psi}\hat{\psi}^*) & \frac{1}{2}\mathrm{Re}(\hat{\varphi}\hat{\theta}^*) & \frac{1}{2}\mathrm{Re}(\hat{\varphi}\hat{\psi}^*) \\ 0 & -\frac{1}{4}(\hat{\varphi}\hat{\varphi}^* + \hat{\psi}\hat{\psi}^*) & \frac{1}{2}\mathrm{Re}(\hat{\theta}\hat{\psi}^*) \\ 0 & 0 & -\frac{1}{4}(\hat{\varphi}\hat{\varphi}^* + \hat{\theta}\hat{\theta}^*) \end{pmatrix} \tag{46}$$

$\bar{T}_{\cdot 2}$ is the same as $\bar{T}_2$ except for the upper two elements of column three, which have a negative sign in $\bar{T}_{\cdot 2}$. The time average of $\vec{w}_2$ follows from (38):

$$\bar{\vec{w}}_2 = \frac{1}{2}\mathrm{Re}\left(\hat{\vec{\alpha}} \times [(\nabla \psi_0)^T(\nabla \hat{\vec{v}}_1^* - \nabla \hat{\vec{v}}_{\cdot 1}^*)] + \frac{1}{2}(\hat{\vec{\alpha}} + \hat{\vec{\alpha}}) \times [(\nabla \nabla \psi_0)(\hat{\vec{v}}_1^* - \hat{\vec{v}}_{\cdot 1}^*)]\right.$$

$$\left. + \frac{1}{2}(\hat{\vec{v}}_1 - \hat{\vec{v}}_{\cdot 1})^T(\nabla \nabla \psi_0)(\nabla \hat{\vec{v}}_1^* - \nabla \hat{\vec{v}}_{\cdot 1}^*) + (\nabla \nabla \phi_1)\hat{\vec{v}}_1^*\right)$$

$$+ \bar{T}_2 \underline{\nabla} \phi_0 + \bar{T}_{\cdot 2} \nabla \psi_0 + (\nabla \nabla \psi_0)(\bar{T}_2 - \bar{T}_{\cdot 2})\underline{\vec{x}} + (\nabla \psi_0)^{\bar{T}}(\bar{T}_2 - \bar{T}_{\cdot 2}). \tag{47}$$

With these expressions and using (8), the time averaged drift force follows from (24) as

$$\overline{\vec{F}_A^{(2)}} = \sum_{panels} \left(p_0 \bar{T}_2 \underline{\vec{n}} + \frac{1}{2}\mathrm{Re}(\hat{p}_1 \hat{\vec{\alpha}}^*) \times \underline{\vec{n}} + \bar{p}_2 \underline{\vec{n}}\right). \tag{48}$$

Correspondingly, the drift moment follows from (27) as

$$\overline{\vec{M}_A^{(2)}} = \sum_{panels} \left[p_0(\underline{\vec{x}} - \underline{\vec{x}}_G) \times (\bar{T}_2 \underline{\vec{n}}) + \frac{1}{2} p_0 \mathrm{Re}\left([\hat{\vec{\alpha}} \times (\underline{\vec{x}} - \underline{\vec{x}}_G)] \times [\hat{\vec{\alpha}}^* \times \underline{\vec{n}}] \right) + p_0 [\bar{T}_2(\underline{\vec{x}} - \underline{\vec{x}}_G)] \times \underline{\vec{n}} \right.$$

$$\left. + \frac{1}{2}\mathrm{Re}(\hat{p}_1 \hat{\vec{\alpha}}^*) \times [(\underline{\vec{x}} - \underline{\vec{x}}_G) \times \underline{\vec{n}}] + \bar{p}_2(\underline{\vec{x}} - \underline{\vec{x}}_G) \times \underline{\vec{n}} \right] \tag{49}$$

The analysis is quite complex. Previously published formulae on that subject and their derivations were much simpler. Reasons for the higher complexity here are:

- The analysis comprises not only the longitudinal force, but all components of the drift force and moment, both in deep and shallow water for all wave directions.

- In favor of higher accuracy, a body-fixed steady disturbance potential (Hachmann method) is used here. Especially in case of shallow water, this necessitates to split the periodic flow potential into two parts ϕ and ψ.
- The present analysis takes into account all second-order terms, not only those which appear most relevant.

The above-given formulae may contain terms which might be omitted without decreasing the accuracy substantially. However, testing the many terms within the formulae for drift force and moment on their relevance under all conditions (ship speed, wave frequency, wave angle, water depth) would be cumbersome and not worthwhile because that would reduce the computing time only by milliseconds per case. Also, the complexity of the program would not be substantially smaller if some terms could be deleted.

As a test for correct formula derivation and programming, $\overline{\vec{F}_A^{(2)}}$ and $\overline{\vec{M}_A^{(2)}}$ were determined using (a) 100 time values per period, and (b) closed formulae based on (48) and (49).

5.3. Drift Force Due to Pressure Acting Between the Average and the Actual Waterline

For the drift force contribution $\vec{F}_B^{(2)}$ due to the variable hull submergence, the second-order pressure at ship-fixed points is irrelevant because it acts on a hull strip along the waterline the breadth of which is a first-order quantity. This breadth is derived from the vertical deviation of the actual from the average waterline designated as $\underline{\zeta}_1$. The breadth may be positive or negative depending on the sign of $-\underline{\zeta}_1$. The following formulae apply to both positive and negative $\underline{\zeta}_1$. In case of a negative breadth, the force and moment contribution A included the hull region between the actual and the mean waterline, which is actually above the water surface; thus, a correction is required also in this case.

On a length element $\underline{\vec{s}}$ along the waterline, the zeroth-order pressure p_0 and the first-order pressure p_1, both at ship-fixed points, produce a drift force element

$$d\vec{F}_B = -\left(p_1 + \frac{1}{2}\underline{\zeta}_1(\nabla p_0)\underline{\vec{t}}\right)\underline{\zeta}_1\ \underline{\vec{s}} \times \underline{\vec{t}}. \tag{50}$$

The expression between the large parentheses is the pressure averaged over the height of the strip between actual and mean waterline. $\underline{\zeta}_1\ \underline{\vec{s}} \times \underline{\vec{t}}$ is the area vector (pointing normal into the hull) between actual and mean waterline corresponding to $\underline{\vec{s}}$. The latter vector is directed forward on starboard and backward on port side. The vector $\underline{\vec{t}}$ (tangential to the hull and having a positive z component on starboard side) is determined from the following conditions:

- $\underline{\vec{t}}\ \underline{\vec{n}} = 0$;
- $\underline{\vec{t}}\ \underline{\vec{s}} = 0$;
- The z component of $\underline{\vec{t}}$ must be 1 to obtain the correct height $\underline{\zeta}_1$ of the relevant strip between actual and mean waterline.

These conditions are satisfied if

$$\underline{\vec{t}} = \frac{\underline{\vec{n}} \times \underline{\vec{s}}}{(\underline{\vec{n}} \times \underline{\vec{s}})_z}, \tag{51}$$

where the index z designates the z component. ∇p_0 follows from (40):

$$\nabla p_0/\rho = (0, 0, g) - \vec{w}_0 \nabla\nabla(\phi_0 + \psi_0). \tag{52}$$

$\underline{\zeta}_1$ is determined from the first-order pressure p_1 at the center of body panels intersected by the average waterline. From the approximation

$$p_1 + (\nabla p_0)\underline{\vec{t}}\,\underline{\zeta}_1 = 0 \tag{53}$$

follows

$$\underline{\zeta}_1 = -p_1/[(\nabla p_0)\underline{\vec{t}}]. \tag{54}$$

The time average of $d\vec{F}_B$ follows from (50) and (54) as

$$\overline{d\vec{F}_B} = -\frac{1}{2}\mathrm{Re}\left[\left(\hat{p}_1 + \frac{1}{2}\underline{\hat{\zeta}_1}(\nabla p_0)\underline{\vec{t}}\right)\underline{\hat{\zeta}_1}^*\right]\underline{\vec{s}} \times \underline{\vec{t}} = -\frac{1}{4}\mathrm{Re}(\hat{p}_1\underline{\hat{\zeta}_1}^*)\underline{\vec{s}} \times \underline{\vec{t}}. \tag{55}$$

The total drift force is obtained as the sum of $\overline{d\vec{F}_B}$ over all body panels intersected by the waterline, using as $\underline{\vec{s}}$ the waterline length segment within each of these panels:

$$\overline{\vec{F}_B^{(2)}} = \sum_{\text{WL panels}} \overline{d\vec{F}_B}. \tag{56}$$

The fluid pressure averaged over the breadth of the strip between actual and average waterline is a first-order quantity. The same holds for the breadth of this strip. Thus, for computing the drift moment element $d\vec{M}_B$, only the zeroth-order lever is relevant. Therefore, the drift moment about the mass center of gravity at $\underline{\vec{x}}_G$ is

$$\overline{\vec{M}_B^{(2)}} = \sum_{\text{WL panels}} (\underline{\vec{x}} - \underline{\vec{x}}_G) \times \overline{d\vec{F}_B}. \tag{57}$$

Due to the limitations of the patch as well as usual panel methods, the pressure can be determined only at the panel centers, not directly at the mean waterline. For the part of p caused by the wave and the diffraction potentials, $\hat{p}$ at the panel center should be multiplied by $e^{k(\underline{z}+d)}$, where k is the wave number and $\underline{z} + d$ is the time-averaged vertical distance between panel center and waterline. For simplification, this correction is applied directly to $\hat{p}_1$ (comprising also other contributions), because in short waves contributions by ship motions are small, and in longer waves, where the ship is moving substantially, the correction is small anyway.

6. Verification

Accurate motion amplitudes are a pre-requisite for computing accurate drift forces. Therefore, Figure 2 compares measured and computed surge, heave and pitch motion amplitudes for a 6500-TEU containership. All results of this and the following two sections are for deep water. The figure shows that the moderately fine hull panel mesh having 1177 partly or fully submerged panels on one ship side needs no refinement. Somewhat larger differences between measured and computed heave amplitudes at medium wave frequencies for Froude numbers around 0.15 are typical. They are caused by heave and pitch resonance, where mass and restoring force and moment nearly cancel, making the motions sensitive to small disturbances and inaccuracies both in experiments and computations.

For a 10.000-TEU containership, Figure 3 shows the non-dimensional coefficient C_{AR} of the added resistance $-F_x$. It is defined as

$$C_{AR} = \frac{-F_x}{\rho g \zeta_A^2 B^2 / L_{pp}}, \tag{58}$$

where ζ_A is wave amplitude and B ship breadth. C_{AR} is plotted over the length ratio parameter

$$\text{LRP} = \sqrt{L_{pp}/\lambda_\infty} = \omega\sqrt{\frac{L_{pp}}{2\pi g}}, \tag{59}$$

where λ_∞ is the wave length in deep water. Waves running from deep into shallow water change their wave length from λ_∞ to $\lambda_\infty \tanh(kD)$, where k is wave number and D is water depth. Thus, to illustrate the effect of shallow water, LRP is defined here using λ_∞, not λ.

Main particulars of the 6500-TEU containership

L_{pp}	286.3 m	B	40.3 m	$T_a = T_f$	13.26 m
V	92,952 m^3	KG	17.996 m	GM	1.079 m
k_{xx}	15.865 m	k_{yy}	68.88 m	k_{zz}	68.55 m

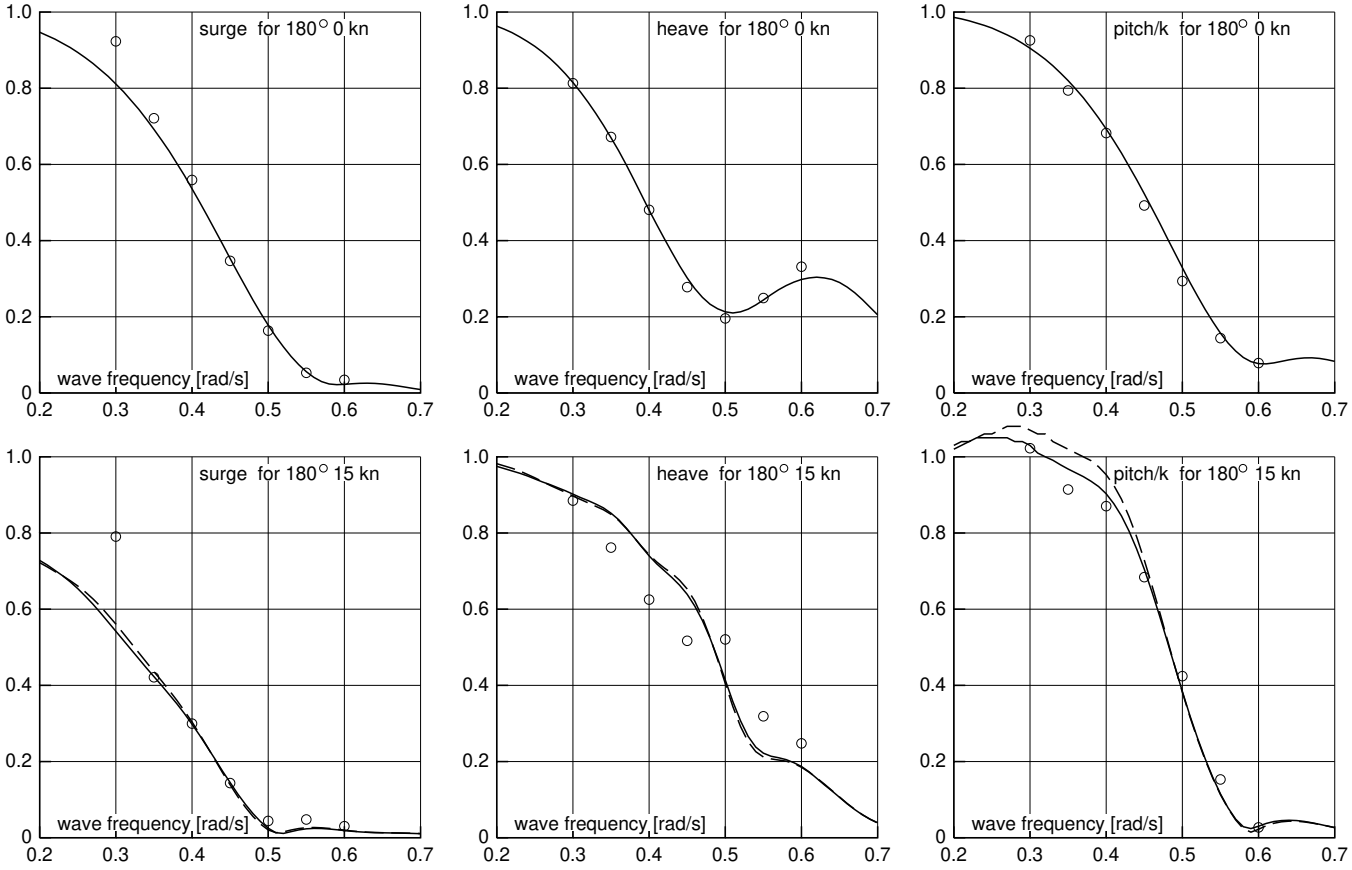

Figure 2. Non-dimensional surge, heave and pitch motion amplitudes of the 6500-TEU containership at zero (**top**) and 15 kn (**bottom**) speed according to experiments of Hong [11] and computations using programs Pansteady and Pandfds: Continuous and broken curves using 1177 and 3379, respectively, partly or fully submerged hull panels on starboard side.

Figure 3 shows results of the present methods Pansteady and Panfds, of the older Rankine panel program GLRankine, as well as results of experiments and RANS calculations. Similarly, Figure 4 shows computed and measured added resistance coefficients for a tanker. For this ship, two different hull panel meshes were used. In the instationary computation for the highest speed, 3590 partly or fully submerged hull panels on both ship sides were used for the 'normal' and 10,364 for the 'fine' hull panel mesh.

The peak of C_{AR} in all curves corresponds to wave lengths causing large heave and pitch motions; it is important for estimating up to which wave conditions a ship can proceed against a heavy seaway, e.g., to avoid stranding. The short-wave region (larger abscissa values) is important for the average fuel consumption in moderate waves. Figure 4 shows

that the added resistance increases substantially with forward speed. In the region of short wavelengths, the added resistance coefficient is larger for full ships (tankers) than for slender (e.g., container) ships with smaller block coefficient. Because the drift force is much smaller than the amplitude of the wave force, both measuring and computing it is difficult, especially in short waves. As shown in Figures 3 and 4, this causes large differences between the results of model experiments (circles), of CFD calculations (triangular and square symbols), and of potential calculations (curves). It is not clear whether present experiments, CFD (RANS) calculations or panel methods can give the most accurate drift forces.

Main particulars of the 10,000 -TEU containership

L_{pp}	321.0 m	B	48.4 m	$T_a = T_f$	15 m
V	140,200 m^3	KG	21.30 m	GM	2.0 m
k_{xx}	19.07 m	$k_{yy} = k_{zz}$	77.23 m	$F_n = 0.183$	

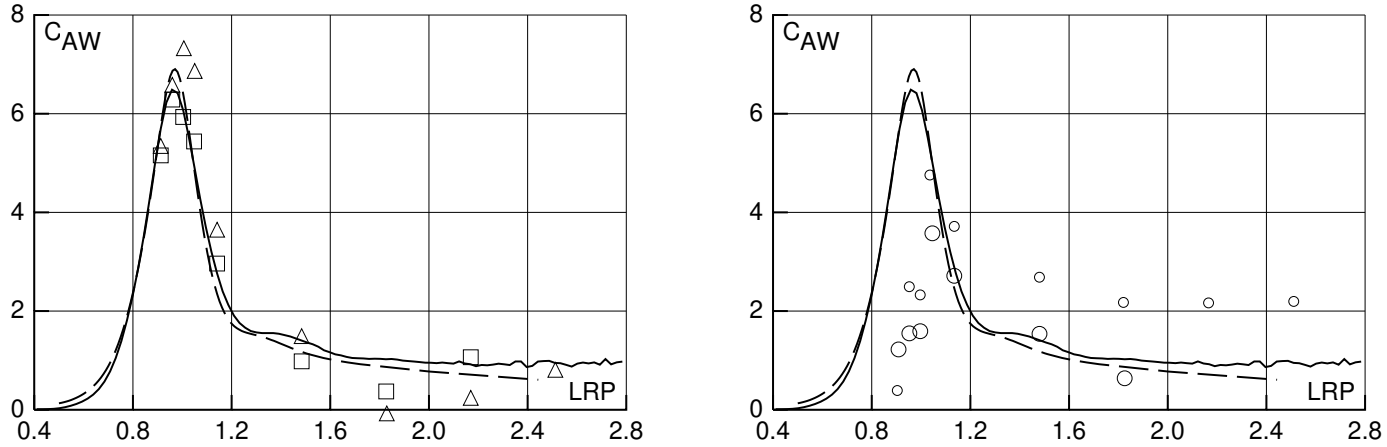

Figure 3. Comparison of added resistance coefficient C_{AR} for a 10,000-TEU containership at 20 knots speed. Curves are results of the programs Panfds (continuous) and the older program GLRankine (broken line). **Left**: Comparison with RANS calculations [12] using a coarse (triangles; 4996 hull panels) and a fine (squares; 10,998 hull panels on both ship sides) grid. **Right**: Comparison with model experiments [12] using two different evaluation methods.

Main particulars of the KVLCC2 tanker

L_{pp}	320.0 m	B	58.0 m	$T_a = T_f$	20.8 m
V	312,600 m^3	KG	18.60 m	GM	5.71 m
k_{xx}	$0.4B$	$k_{yy} = k_{zz}$	$0.25L_{pp}$		

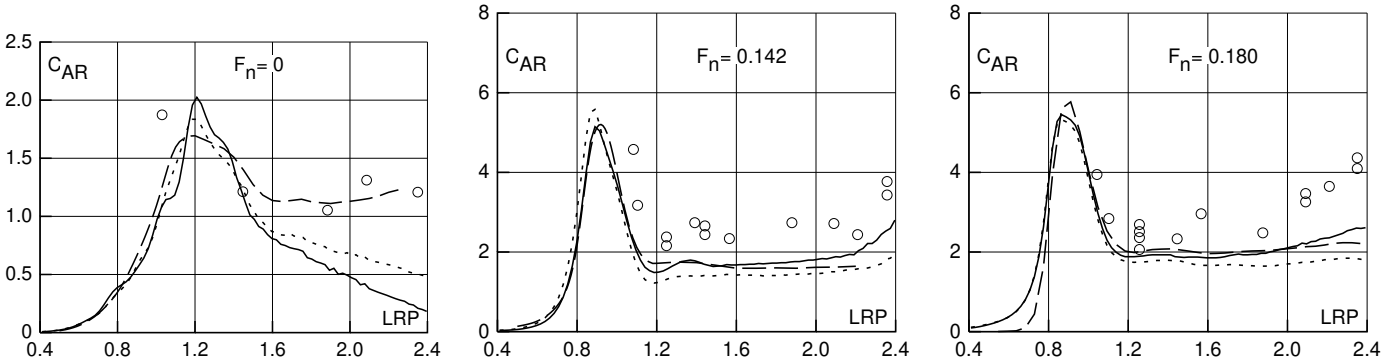

Figure 4. Comparison of added resistance coefficient C_{AR} of the KVLCC2 tanker for three different Froude numbers F_n. Curves are results of the programs Panfds using a normal (continuous) or a very fine body panel mesh (dotted curves); broken curves show results of the older program GLRankine; and markers designate results of model experiments by Bingje and Steen [13].

7. Influence of the Wave Angle

Figure 5 shows the added resistance coefficient of the KVLCC2 tanker as a function of the length ratio parameter LRP for different wave angles. For wave lengths $< L_{pp}$, wave angles 150 and 120 degrees often cause higher added resistance than head waves. The negative peaks in long waves of angles 90, 60 and 30 degrees at 15 knots are caused by roll resonance.

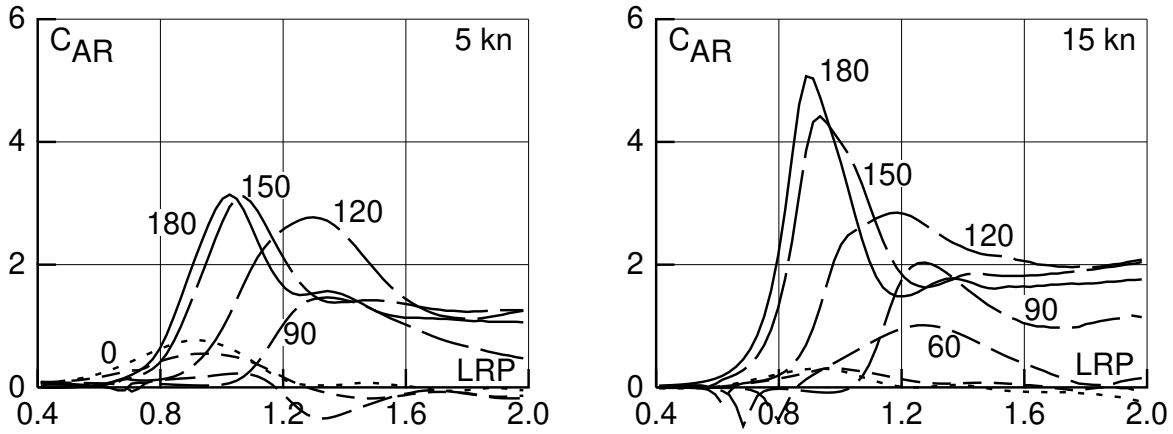

Figure 5. Added resistance coefficient C_{AR} of the KVLCC2 tanker for speeds 5 and 15 knots, plotted over the length ratio parameter LRP. Continuous curves for wave angle 180 degrees (head waves), progressively shorter broken curves for wave angles 150, 120, 90, 60, 30 and 0 degrees.

8. Transverse Force and Yaw Moment

For steering in oblique and transverse waves, the transverse drift force F_y and the yaw drift moment M_z may be important. They will be characterized here by the non-dimensional coefficients

$$C_{Fy} = \frac{-F_y}{\rho g \zeta_A^2 L_{pp}} \tag{60}$$

and

$$C_{Mz} = \frac{-M_z}{\rho g \zeta_A^2 L_{pp}^2}. \tag{61}$$

For oblique waves, C_{Fy} is positive if the force is directed to wave lee side, and C_{Mz} if the moment is turning the bow to wave lee side; for exactly head and following waves, both coefficients are zero.

Figures 6 and 7 show the dependence of C_{Fy} and C_{Mz}, respectively, on wave frequency and direction, again for the KVLCC2 tanker at two different speeds. The maximum of the transverse force occurs for waves from the side. The yaw drift moment changes sign depending on wave length for most of the wave angles. Again, spikes at low frequencies are caused by resonant roll motion. To illustrate the effect of higher Froude numbers for a slender ship, Figure 8 shows the drift force and moment coefficients for the 6500-TEU containership at 20 knots speed. The spikes at high frequencies, especially for the wave angle 90 degrees, are caused by deficiencies of the numerical method.

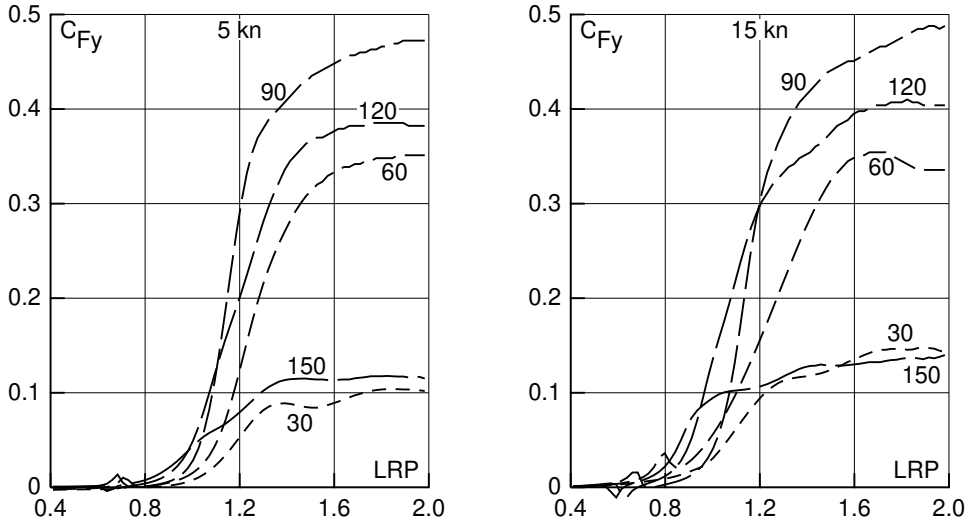

Figure 6. Transverse drift force coefficient of the KVLCC2 tanker for speeds 5 and 15 knots, plotted over the length ratio parameter LRP, for wave angles 150 (longest curve segments), 120, 90, 60 and 30 degrees (progressively shorter curve segments).

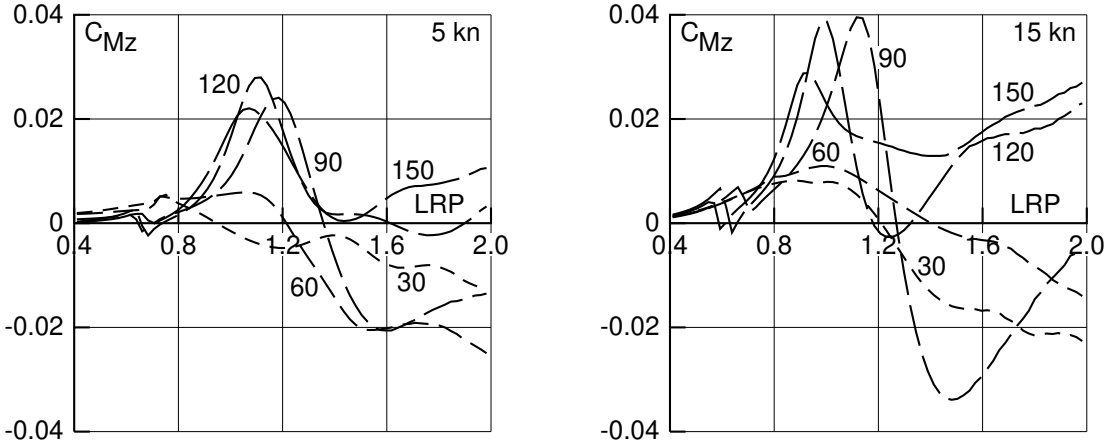

Figure 7. Yaw drift moment coefficient of the KVLCC2 tanker for speeds 5 and 15 knots, plotted over the length ratio parameter LRP, for wave angles 150 (longest curve segments), 120, 90, 60 and 30 degrees (progressively shorter curve segments).

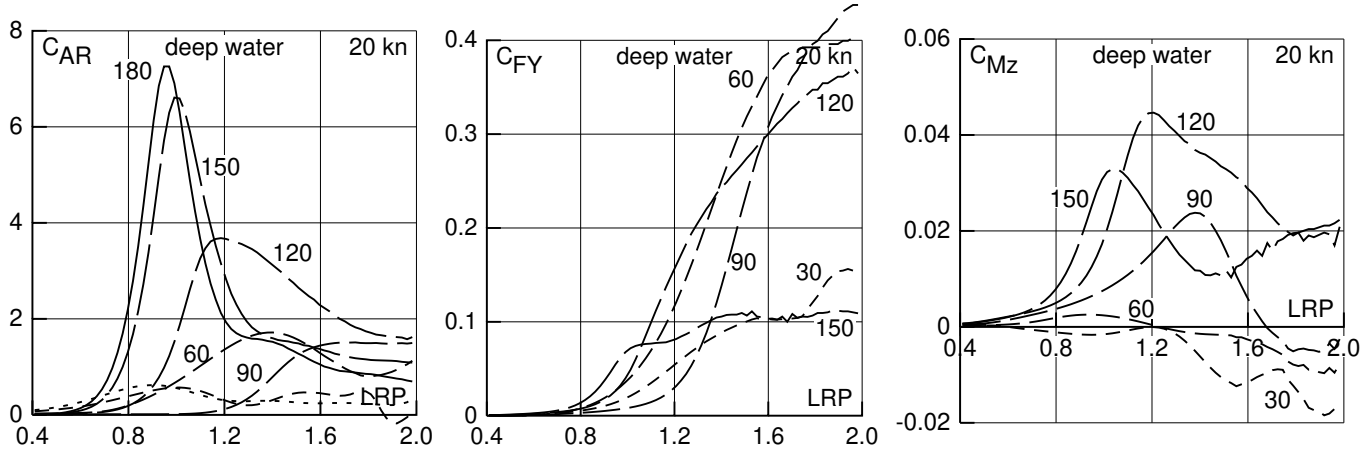

Figure 8. Coefficients of added resistance, transverse drift force and yaw drift moment of the 6500-TEU containership at 20 knots speed, plotted over the length ratio parameter LRP. Continuous curve for wave angle 180 degrees, progressively shorter curve segments for angles 150, 120, 90, 60, 30 and 0 degrees.

9. Influence of Water Depth

Figures 9 and 10 illustrate the coefficients of added resistance, transverse force and yaw moment for water depths of 50 m and 25 m, respectively. Generally, positive drift forces and moments are larger and negative ones are smaller (more negative) in shallow water than in deep water. The main reason for that is because in shallow water waves, amplitudes of horizontal velocities in the direction of wave propagation are larger than those in vertical direction by the factor $1/\tanh(kD)$. Thus, for constant wave amplitude and frequency, horizontal velocities increase if the water depth decreases. For estimating the ship's ability to proceed and turn in waves, shallow water is decisive if $\tanh(kD)$ is substantially smaller than 1. In the present case, the effect is moderate for 50 m and large for 25 m water depth.

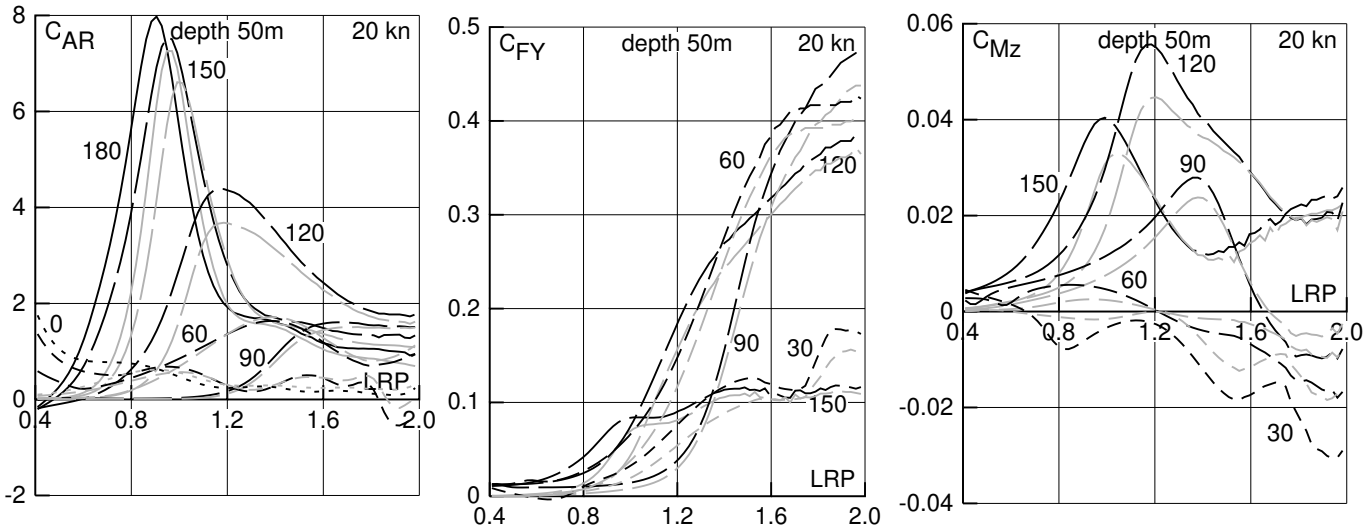

Figure 9. Coefficients of added resistance, transverse drift force and yaw drift moment of the 6500-TEU containership at 20 knots speed, plotted over the length ratio parameter LRP. Continuous curve for wave angle 180 degrees, progressively shorter curve segments for angles 150, 120, 90, 60, 30 and 0 degrees. Black for water depth 50 m, gray for deep water.

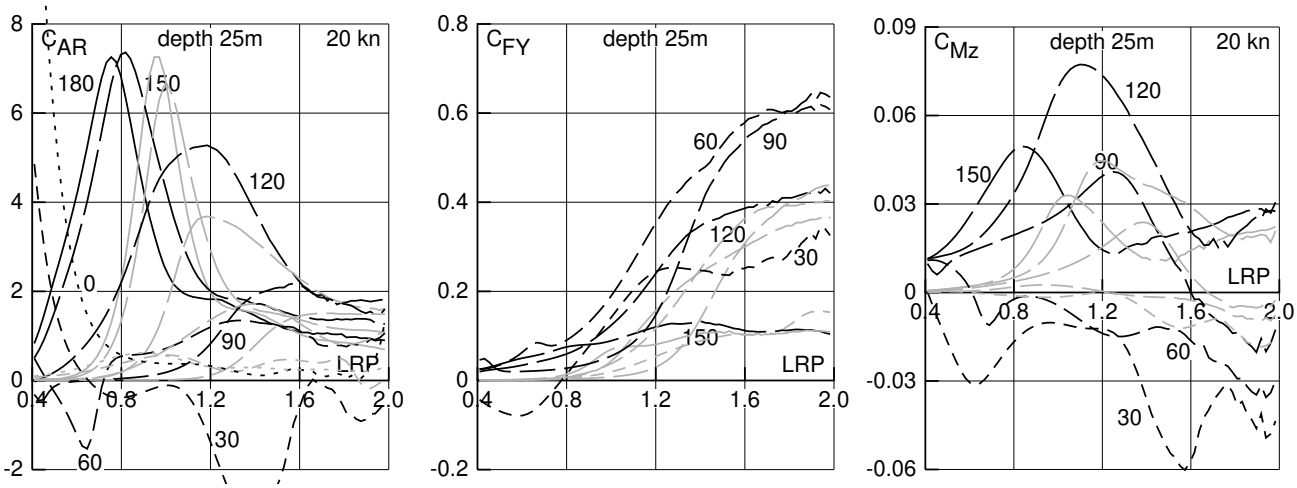

Figure 10. Like Figure 9, but for 25 m water depth.

Corresponding calculations were made for water depths of 20 m and 17 m. Results showed that, for these depths, a speed of 20 kn is excessive. For 17 m water depth, the draft increases from 13.26 m at rest to 15.07 m at a speed of 20 kn, and the forward trim increases from zero to 1.06 m, possibly causing yaw instability. Further, the roll damping becomes negative; thus, the ship will execute roll motions at its roll eigenfrequency even without

waves. (Note that the metacentric height used in the tests and in the present calculations is only GM = 1.079 m.)

In Figures 11–14, results for a speed of 5 kn in deep water and in water of 50 m, 25 m and 17 m depth are shown. This speed may be considered for estimating the danger of insufficient maneuverability in heavy weather near to a shore. In this case, a water depth of 50 m has only small effect on drift force and moment, 25 m depth has a moderate effect, and 17 m depth a large effect, especially on the transverse force and the yaw moment.

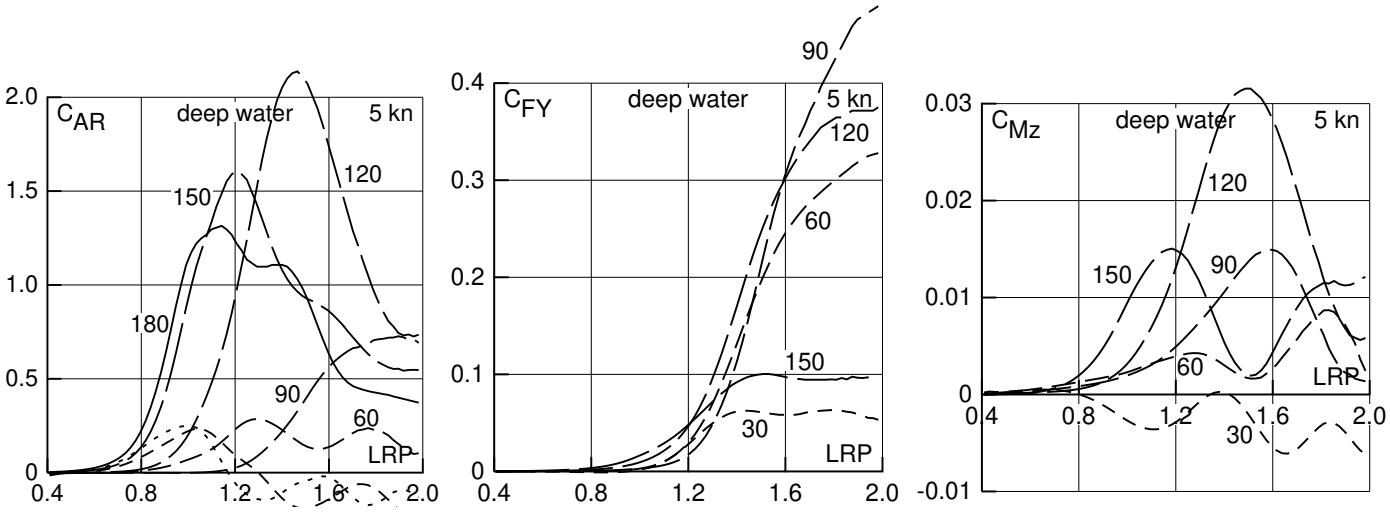

Figure 11. Coefficients of added resistance, transverse drift force and yaw drift moment of the 6500-TEU containership at 5 knots speed, plotted over the length ratio parameter LRP. Continuous curve for wave angle 180 degrees, progressively shorter curve segments for angles 150, 120, 90, 60, 30 and 0 degrees.

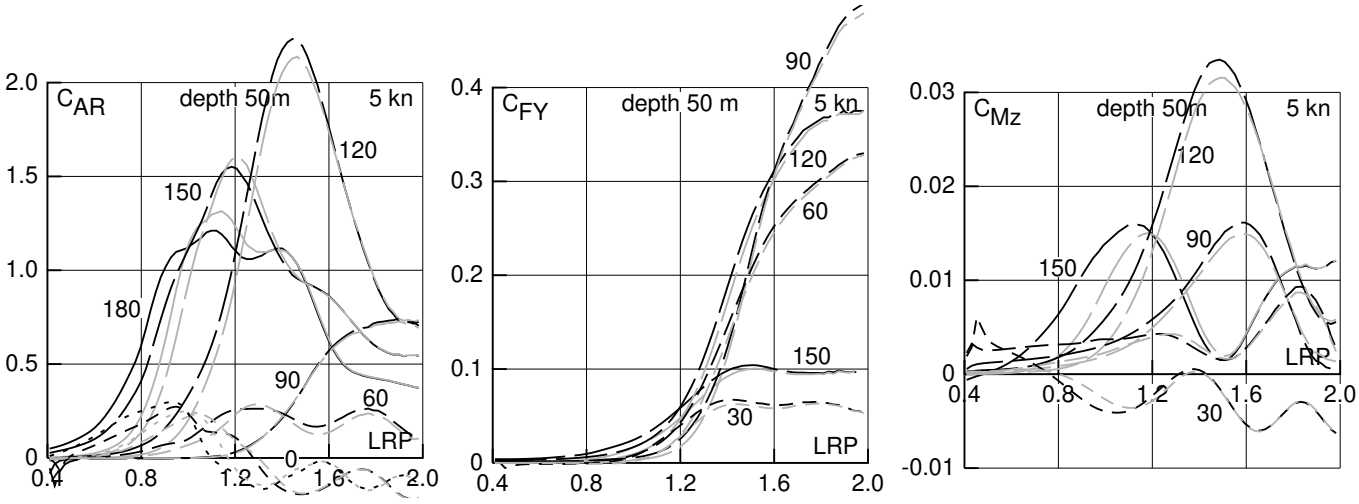

Figure 12. Like Figure 11, but for 50 m water depth (black) and for deep water (gray).

The added resistance per squared wave amplitude is not always maximum in head waves. For 20 kn speed in shallow water, the maximum is a little higher for 150 than for 180 degrees (Figure 10), whereas at a speed of 5 kn, the maximum is much higher for wave angles of 120 than for 180 degrees (Figures 11–14); results for wave angle 150 degrees are in between. On the other hand, for the containership at both speeds and for all water depths, the transverse drift force is maximum for 90 degrees, and the yaw moment for 120 degrees wave angle.

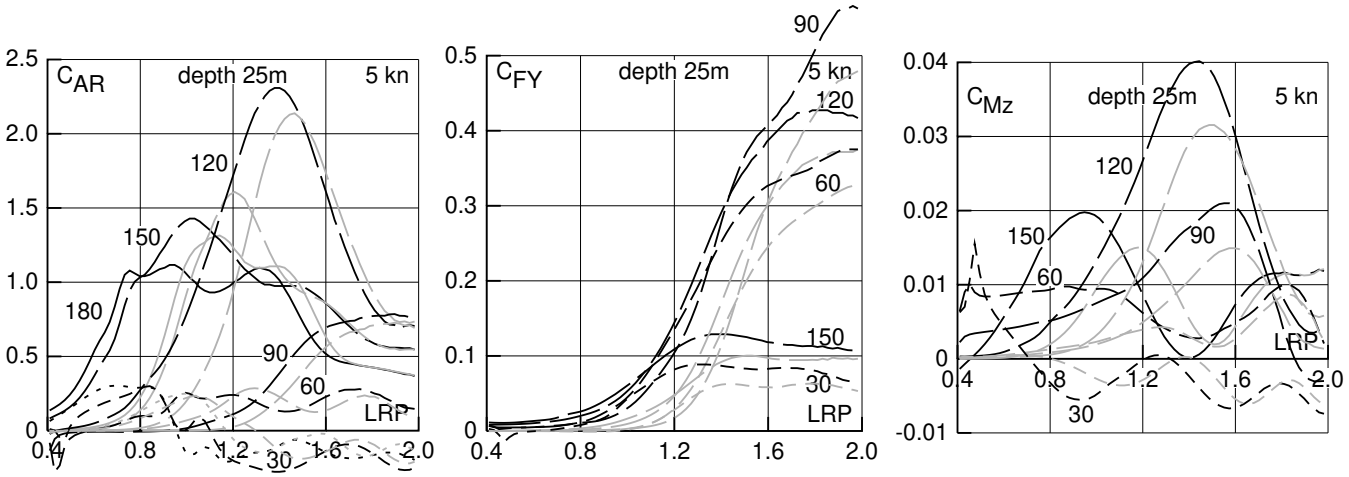

Figure 13. Like Figure 11, but for 25 m water depth (black) and for deep water (gray).

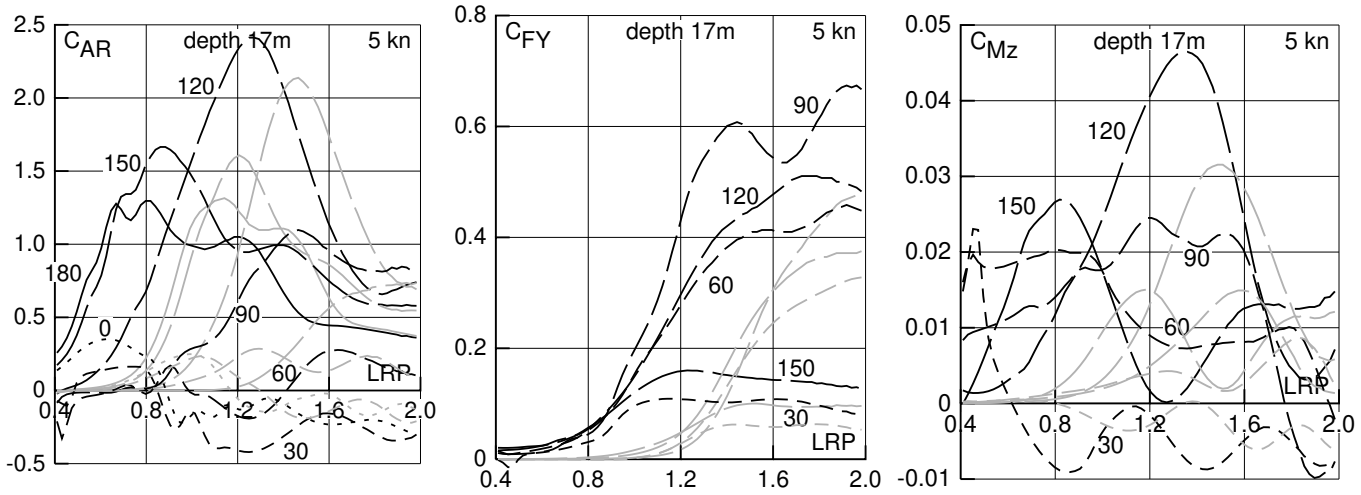

Figure 14. Like Figure 11, but for 17 m water depth (black) and for deep water (gray).

10. Conclusions

According to the present computations for small speed in deep water, the added resistance in oblique waves may be nearly two times that in head waves (Figure 11). For shallow water, that ratio is even larger (Figures 12–14). Drift forces at low speed are relevant for estimating the danger of stranding in adverse weather conditions. The same holds for the transverse drift force and the corresponding yaw moment in oblique or transverse waves. Thus, the methods elaborated here for computing the wave drift force and moment for arbitrary wave direction on deep and shallow water appear practically relevant. The method may help also to correct the wave influence in speed runs and maneuvering tests during trial trips.

To further validate the method, comparisons with results of model experiments or CFD calculations of wave drift forces and moments on deep and shallow water would be helpful.

Funding: This research received no funding.

Data Availability Statement: Please contact the author.

Conflicts of Interest: I declare that there is no conflict of interest.

Appendix A. Determination of the Hesse Matrix of Potentials

To determine the first-order flow pressure p_1, one needs to know the Hesse matrix $\nabla\nabla\phi_0$ (in shallow water also that of ψ_0) of the steady disturbance potential ϕ_0 due to the mean forward speed on the wetted body surface if one does not use the Hachmann method. But even if this method is used, the Hesse matrices of ϕ_1 and ψ are required to determine the drift force and moment. Their contribution to added resistance is moderate.

Panel methods result, in the limit of vanishing panel size, in correct values for the first derivatives of the potential only at the panel centers, not at arbitrary points. The patch method, on the other hand, approximates only averages of first derivatives over panels. Thus, second derivatives cannot simply be determined as analytical derivatives of the panel or patch approximations of the potential.

Useful approximations for the second derivatives are determined, instead, as finite differences between first derivatives sampled at the centers of the neighbor panels of the panel of interest O. For a triangular body panel having three neighbor panels, the midpoints of the neighbors are designated as A, B and C (Figure A1). If a panel O intersects the waterline, and if only one of its vertices is below the waterline, O is used instead of the missing neighbor panel. Figure A2 shows which panels are then used as the other neighbors. The best accuracy is attained if the neighbor panel centers A, B and C approximate an equilateral triangle.

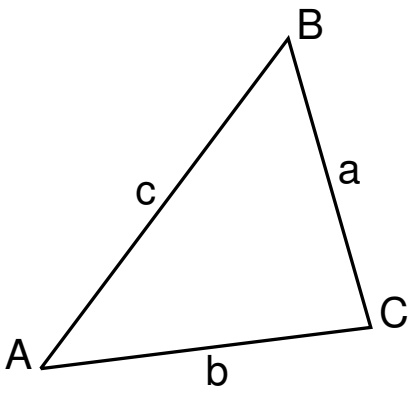

Figure A1. Centers of direct neighbor panels A, B, C and meaning of vectors a, b and c.

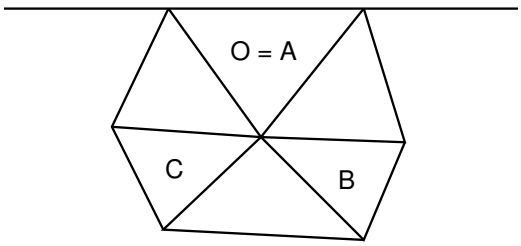

Figure A2. Selection of neighbor panels A, B, C to the panel of interest O if O has less than three at least partly submerged neighbors.

The Hesse matrix of a panel O is defined as

$$\nabla\nabla\phi = \nabla\vec{u} = \begin{pmatrix} u_{1x} & u_{1y} & u_{1z} \\ u_{2x} & u_{2y} & u_{2z} \\ u_{3x} & u_{3y} & u_{3z} \end{pmatrix}, \tag{A1}$$

where 1, 2, 3 indicate components of the velocity $\vec{u}$, and x, y, z partial derivatives in the coordinate directions. The fluid velocities $\vec{u}_A$, $\vec{u}_B$ and $\vec{u}_C$ at the midpoints of the neighbor

panels are supposed to be known. Defining $\vec{a} = \vec{x}_C - \vec{x}_B$ and $\vec{b} = \vec{x}_A - \vec{x}_C$ (Figure A1), the following five relations are used to determine the elements of the Hesse matrix:

$$(\vec{a} \cdot \nabla)\vec{u} = \vec{u}_C - \vec{u}_B; \tag{A2}$$

$$(\vec{b} \cdot \nabla)\vec{u} = \vec{u}_A - \vec{u}_C; \tag{A3}$$

$$\vec{a} \cdot \mathrm{rot}\vec{u} = 0; \tag{A4}$$

$$\vec{b} \cdot \mathrm{rot}\vec{u} = 0; \tag{A5}$$

$$\mathrm{div}\vec{u} = 0. \tag{A6}$$

The first two of these equations (i.e., six scalar equations) are finite-difference equations for $\nabla\vec{u}$ in directions tangential to the hull surface. The following three scalar equations ensure the correct change of $\vec{u}$ in the direction normal to the hull. All together, the nine scalar equations form a linear equation system for the nine elements of the matrix (A1). Because the Hesse matrix is symmetric, the result can perhaps be improved by taking the average of the original solution and its transpose.

References

1. Shigunov, V. Assessment of Manoeuvrability in Waves. *J. Ship. Res.* **2019**, *63*, 76–93. [CrossRef]
2. IMO. *Draft Revised Guidelines for Determining Minimum Propulsion Power to Maintain the Manoeuvrability of Ship in Adverse Conditions*; Paper MEPC 71/INF 28 submtted by Denmark, Germany, Japan, Spain and IACS; IMO: London, UK, 2017.
3. Blendermann, W. *Practical Ship and Offshore Structure Aerodynamics*; TU Hamburg, Schriftenreihe Schiffbau: Hamburg, Germany, 2014; ISBN 978-3-89220-669-9.
4. Uharek, S.; Cura-Hochbaum, A. Power prediction for safe Manoeuvring in Waves. In Proceedings of the 32nd Symposium on Naval Hydrodynaamics, Hamburg, Germany, 5–10 August 2018.
5. El Moctar, B.O.; Schellin, T.E.; Söding, H. *Numerical Methods for Seakeeping Problems*; Springer: Cham, Switzerland, 2021; ISBN 978-3-030-62561-0.
6. Söding, H.; Jensen, G.; Mi, Z.-X., Rankine source sethods for numerical solutions of the steady wave resistance problem. In Proceedings of the 16th Symposium on Naval Hydrodynamics, Berkeley, CA, USA, 13–16 July 1986.
7. Söding, H. A method for accurate force calculations in potential flow. *Ship Technol. Res.* **1993**, *40*, 176.
8. Söding, H.; von Graefe, A.; El Moctar, O.; Shigunov, V. Rankine source method for seakeeping predictions. In Proceedings of the ASME 2012 31st International Conference on Ocean, Offshore and Arctic Engineering, Rio de Janeiro, Brazil, 1–6 July 2012; OMAE2012-83450.
9. Hachmann, D. Calculation of pressures on a ship's hull. *Ship Technol. Res.* **1991**, *38*, 111–1333.
10. Von Graefe, A. A Rankine Source Method for Ship-Ship Interaction and Shallow Water Problems. Ph.D. Thesis, University of Duisburg-Essen, Essen, Germany, 2014.
11. Hong, S.Y. Wave induced loads on ships, joint industry project—II. In *Technical Report BSPIS503 A-2207-2 (Confidential)*; MOERI: Daejeon, Republic of Korea, 2010.
12. Söding, H.; Shigunov, V.; Schellin, T.; el Moctar, O. A Rankine panel method for added resistance of ships in waves. In Proceedings of the ASME 2012 31st International Conference on Ocean, Offshore and Arctic Engineering, Rio de Janeiro, Brazil, 1–6 July 2012; OMAE2012-83457.
13. Bingje, G.; Steen, S. Added resistance of a VLCC in short waves. In Proceedings of the 29th International Conference on Ocean, Offshore and Arctic Engineering, Shanghai, China, 6–11 June 2010.